Simple Fluorescence Sensing Approach for Selective Detection of Fe³⁺ Ions: Live-Cell Imaging and Logic Gate Functioning

Puthiyavalappil Rasin, Vipin Manakkadan,
Vishnunarayanan Namboothiri Vadakkedathu Palakkeezhillam, Jebiti Haribabu, Cesar Echeverria,
and Anandaram Sreekanth*

ACCESS | Metrics & More | Article Recommendations | SI Supporting Information

ABSTRACT: A pyrene-based fluorescent chemosensor APSB [*N*-(pyrene-1-ylmethylene) anthracen-2-amine] was designed and developed by a simple condensation reaction between pyrene carboxaldehyde and 2-aminoanthracene. The APSB fluorescent sensor selectively binds Fe^{3+} in the presence of other metal ions. Apart from this, APSB shows high selectivity and sensitivity toward Fe^{3+} ion detection. The detection limit for APSB was 1.95 nM, and the binding constant (K_b) was obtained as 8.20×10^5 M^{-1} in DMSO/water (95/5, v/v) medium. The fluorescence quantum yields for APSB and APSB−Fe^{3+} were calculated as 0.035 and 0.573, respectively. The function of this fluorescent sensor APSB can be explained through the photo-induced electron transfer mechanism which was further proved by density functional theory studies. Finally, a live-cell image study of APSB in HeLa cells was also carried out to investigate the cell permeability of APSB and its efficiency for selective detection of Fe^{3+} in living cells.
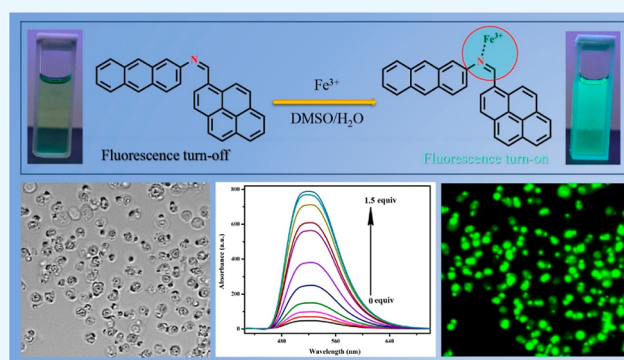
INTRODUCTION

The development of facile and selective chemosensors for different transition metal ions has gained considerable attention due to their potential applications in chemical and biological streams.[1−3] Chemosensors can be either organic or inorganic compounds that are capable of selectively detecting the metal ion of interest with the change of associated properties. Different types of chemosensors have been produced till date. Among them, fluorescent chemosensors display advantages in the sensing of metal ions over other spectroscopic techniques such as atomic absorption spectroscopy and inductively coupled plasma mass spectroscopy owing to their precision with high sensitivity and real-time detection.[4,5] Nowadays, the sensors which are active in light have gained more attraction due to their simple working mechanism which is based on the interaction between the chemosensor and the metal ions. In addition, intramolecular charge transfer, chelation enhanced fluorescence, photo-induced electron transfer (PET), and charge transfer from the chelator to the fluorophore are the common mechanisms associated with metal ion sensing study.[6−8]

Iron is an essential element for cellular physiology.[9] Iron intake is very crucial since iron deficiency and iron overload in the human body can cause potential health disturbances. Iron deficiency is the most common condition that affects almost 500 million people around the world.[10] The impact of iron

deficiency can vary from severe anemia to cognitive impairment and neurobehavioral disorders in children.[11] However, iron overload can lead to many pathological conditions such as liver disease, heart disease, cancer, diabetes, development of abnormal immune system, and neurodegenerative disorders.[12−14] Hence, these circumstances demand selective, sensitive, and facile sensors for the effective detection of Fe^{3+} ions mainly in drinking water. Different techniques can be employed to determine iron concentration based on its chemical properties. Even though many sophisticated instruments are there for determining the iron concentration both quantitatively and qualitatively, several restrictions are associated with them including very high cost, the need for experts to handle the instruments, maintaining ambient conditions, and so forth.

Pyrene compounds are comprised of four benzene rings resulting in a fused aromatic system. Generally, pyrene is a fluorescent probe whose emission is sensitive to the o polarity of the solvent or the environment.[15] Hence, pyrene-based
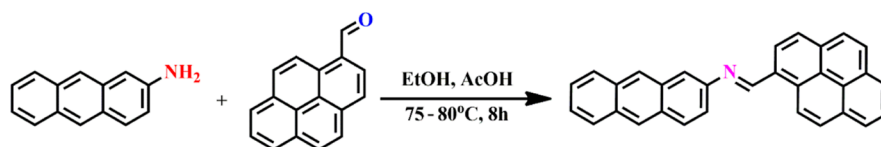
Scheme 1. Synthesis of Sensor APSB

compounds can be considered an ideal template for the development of novel fluorescent receptors for metal ions due to their unique photophysical properties such as emission wavelengths extended to the visible region, a large absorption coefficient, and a high fluorescence quantum yield.[16] Similarly, several fluorescent sensors based on nanomaterials for the detection of various metal ions are already described in previous literature. Comparing to organic compound-based sensors, nanomaterial-based fluorescent sensors have some limitations such as poor photo stability, stability issues in aqueous environment, and lack of selectivity of metal ions in sensing application.[17] Apart from this, most of the graphene-based nanocomposites for metal ion sensing require harsh chemical synthesis with low yield.[18] Toxicity and agglomeration of nanoparticles usually make them less preferable in metal ion sensing based on their fluorescent properties.[19] Even though gold nanoparticles have excellent applications in various fields, their high cost of preparation make them less suitable candidates for metal ion sensing. Considering all these facts into account, in this study, we report a pyrene-based chemosensor capable of detection of Fe^{3+} ions in an aqueous medium. The cost of synthesis of the chemosensor is comparatively low and shows high selectivity and sensitivity toward Fe^{3+} ions. The preparation method of the chemosensor is very facile and takes only a couple of hours. Also, this chemosensor is free from the limitations described above in the case of fluorescent based nanomaterials which recommends the use of as-synthesized pyrene-based fluorescent sensors for the selective recognition of Fe^{3+} ions.

The fluorescent chemosensor has been synthesized by condensing pyrene carboxaldehyde with 2-amino anthracene leading to a new pyrene-anthracene hybrid system [N-(pyrene-1-ylmethylene) anthracen-2-amine (APSB)]. The chemosensor APSB can selectively detect Fe^{3+} ions in DMSO/water media (95/5, v/v) over the presence of other 14 metal ions. The chemosensor was well characterized by UV–vis, nuclear magnetic resonance (NMR), and ESI-MS techniques. The sensing mechanism of the chemosensor APSB–Fe^{3+} complex was further confirmed by density functional theory (DFT) and FT-IR spectral studies. The live-cell imaging studies of the chemosensor APSB in HeLa cells were also carried out to investigate the practical application of the chemosensor.

■ EXPERIMENTAL SECTION

Synthesis of Chemosensor APSB. The chemosensor APSB has been synthesized by adopting and modifying a reported procedure.[20] The synthetic procedure and NMR, high-resolution mass spectroscopy, and other related spectra (Figures S1–S3) which confirm the structure of the compound are discussed in the Supporting Information.

Preparation of Stock Solution of APSB and Metal Ions. All desired metal ion solutions were prepared in freshly double-distilled water which was free from other metal ions and any other impurities. The stock solution was prepared by

dissolving 0.0041 g of APSB (1×10^{-3} M) in a DMSO/water solvent system (95/5, v/v). To conduct fluorescence spectral studies, all metal ion solutions were further diluted to 1×10^{-5} M concentration. Chloride salts of all metal ions have been chosen for this study. The metal ion selective study was carried out using APSB (1 μL, 1×10^{-3} M in 3 mL of DMSO/water solvent) and different chloride salts of metal ions (1 μL, 1×10^{-3} M in 3 mL of DMSO/water solvent) at a pH of 8. All experiments were conducted at room temperature.

Detection Limit and Binding Constant Calculations. The formula $3\sigma/K$, where σ is the standard deviation of the blank measurement and K is the slope derived from the plot of fluorescence intensity versus Fe^{3+} ion concentrations, was used to calculate the detection limit.[21] A better linear relationship of the fluorescence intensity versus Fe^{3+} concentration at 520 nm was found in the $4-10.5 \times 10^{-7}$ M range ($R^2 = 0.9892$, Figure S4). The detection limit of Fe^{3+} was found to be 1.95 nM. The K_a value was determined from the plot of $1/(I - I_0)$ against $1/[Fe^{3+}]$.[22]

Cell Imaging Studies. To investigate the use of the sensor APSB to detect Fe^{3+} ions in biological systems, fluorescence imaging study was carried out. Before this study, cell toxicity study was performed using a general method known as the MTT (3-(4,5-dimethylthiazol-2-yl)-2,5-diphenyl-2H-tetrazolium bromide) assay technique.[23−25] The test was conducted after incubating the HeLa cells with the sensor APSB at different concentrations (0−50 μM) for 12 h. HeLa cells were seeded in 12-well plates in complete media and cultured for 12 h under 5% CO_2 at 37 °C. The cells were slowly washed three times with phosphate-buffered solution (PBS) to eliminate excess Fe^{3+}. After that, the cells were treated with APSB (10 μM) for 10 min. In the next step, the cells were gently washed three times with PBS to eliminate traces of APSB and culture media. Formaldehyde solution (3.7%, pH 7.0) was used to fix the cells, and images of cells were recorded by a fluorescence microscope.

Theoretical DFT Studies. Computational DFT calculations of the sensor APSB and APSB–Fe^{3+} complex have been performed to investigate and analyze the electronic properties of the individual atoms using B3LYP/6-311G(d,p), LANL2DZ level theories. Also, a molecular electrostatic potential (MEP) map study was carried out to predict the chemical reactivity and energy levels [highest occupied molecular orbital (HOMO) and lowest unoccupied molecular orbital (LUMO)] associated with this reaction.

■ RESULTS AND DISCUSSION

Synthesis of APSB. The sensor APSB was synthesized via a simple Schiff base reaction, which is described in Scheme 1. In brief, an imine (compound 3) was obtained by the condensation reaction between pyrene carboxaldehyde and 2-aminoanthracene in a DMSO/water solvent system (95/5, v/v) in the presence of a couple of drops of glacial acetic acid as the catalyst. The sensor APSB was prepared with an excellent yield (92%).
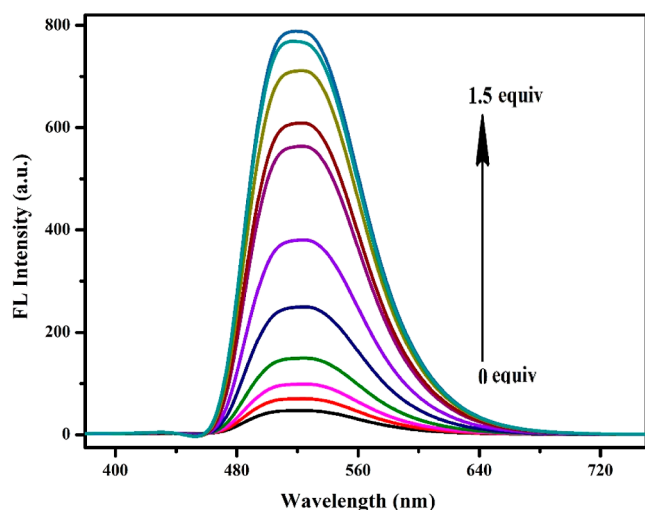
Figure 1. Fluorescence emission spectra of APSB (1×10^{-5} M) with the incremental addition of Fe^{3+} in DMSO/water (95/5, v/v) solution (λ_{em} = 520 nm).
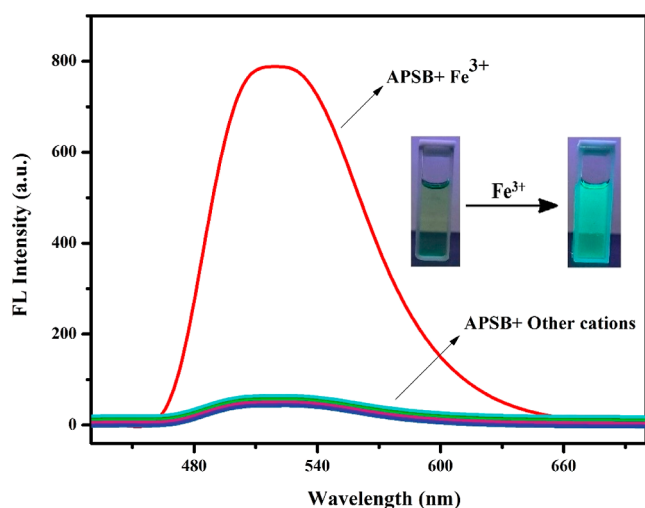

Figure 2. Fluorescence emission pattern of sensor APSB (1×10^{-5} M) in DMSO/water (95/5, v/v) with different metal ions (1×10^{-3} M), λ_{em} = 520 nm; inset: APSB with Fe^{3+} under xenon lamp in the dark atmosphere.

Solvatochromism. The synthesized sensor APSB is completely soluble in DMSO and DMF solvents. Hence, the sensor was diluted into DMSO and DMF solvents (solvent/ H_2O: 95/5, v/v), and the UV−vis spectral studies were studied at room temperature. The spectra described major absorption peaks around 265−295 and 365−430 nm (Figure S5). Due to the polarity difference in the solvent systems, a bathochromic shift of absorption peaks was observed. The intensity of the absorption peak of APSB is maximum in a polar aprotic solvent DMSO/water (95/5, v/v), and this solvent system was selected for further studies. The absorption wavelength of 413 nm was chosen for further fluorescence investigation.

Time-Dependence Study. Time-dependence study was also carried out using fluorescence spectrophotometry to use the sensor APSB for practical application toward the sensing of Fe^{3+} ions. To perform this study, the sensor APSB was added to Fe^{3+} ions, and fluorescence spectra were recorded at regular intervals of time (0−20 min) (Figure S6). The results described that there was no significant variation in the

fluorescence intensity over various time intervals, suggesting APSB as a rapid tool for the detection of Fe^{3+} ions with a response time of 3 min.

pH Study. To investigate the effect of pH on Fe^{3+} ion sensing, a pH study was carried out within the range of 1 to 14. The pH of the medium was adjusted by hydrochloric acid and sodium hydroxide solutions. The fluorescence emission intensity of the sensor APSB (1×10^{-5} M) was almost constant in the range from pH = 1 to pH = 14, revealing its consistency. The fluorescence emission intensity of the APSB−Fe^{3+} complex in an acidic medium was low and gradually increases when the pH of the medium shifts from acidic to neutral, and the intensity reaches a maximum at the pH of 8, as shown in Figure S7. Also, the fluorescence intensity of the APSB−Fe^{3+} complex decreases gradually after pH 10. Hence, the overall outputs of the pH study describe that the sensor APSB acts as a selective detector for Fe^{3+} ions under physiological pH, which reveals the compatibility of the sensor toward biological applications.

Fluorescence Spectral Studies of Sensor APSB. To investigate the selectivity of the synthesized compound, first, we examined the sensing ability of sensor APSB. The excitation wavelength was fixed at 413 nm based on the maximum absorption wavelength of the sensor before starting the fluorescent measurements. The binding ability of the sensor APSB with different metal ions was studied in DMSO/water and DMF/water (95/5, v/v) solvent systems. The fluorescence emission of the sensor APSB in the DMF/water (95/5, v/v) medium was weak compared to its emission in DMSO/water (95/5, v/v) system. Also, the solvent DMF itself can form a complex with Fe^{3+} ions,[26] which can further interfere in the fluorescent studies of the sensor APSB. Their results described that the detection of Fe^{3+} ions by the sensor APSB was solvent-dependent. From the structure of the sensor APSB, it was predicted that the imine nitrogen attracts Fe^{3+} ions. Therefore, the sensor APSB was studied for its sensing property toward different metal ions (Co^{2+}, Cr^{3+}, Cu^{2+}, Fe^{2+}, Hg^{2+}, Pb^{2+}, Ga^{3+}, Ni^{2+}, Mg^{2+}, Cd^{2+}, Ca^{2+}, Mn^{2+}, Al^{3+}, Zn^{2+}, Sn^{2+}, and Sn^{4+}) in DMSO/water (95/5, v/v) medium. The fluorescence spectral changes of the sensor APSB in the presence of different metal ions are described in Figure 2. The sensor APSB shows a characteristic emission peak at a wavelength of 520 nm, which corresponds to the monomer emission intensity of APSB. After the addition of various metal ions (1×10^{-3} M) in APSB (1×10^{-5} M), the fluorescence emission was not affected significantly. However, the addition of Fe^{3+} ions to the sensor APSB introduced a drastic enhancement in the emission intensity. The fluorescence emission intensity was 17-fold higher than that of bare APSB at 520 nm. The color change observed upon addition of Fe^{3+} ions to the sensor APSB under a xenon lamp (75 W) in a dark atmosphere is shown as an inset in Figure 2. The UV−vis absorption studies of the sensor APSB revealed similar spectral changes (Figure S8). These results suggested that the sensor APSB has a good binding affinity toward Fe^{3+} and the least binding affinity toward other studied metal ions.

Fluorescence titration experiments were carried out to have a better understanding of the interaction of the sensor APSB and Fe^{3+} ions at the molecular level. The fluorescence emission intensity gradually increased upon the incremental addition of Fe^{3+} ions to APSB in a DMSO/water (95/5, v/v) medium as depicted in Figure 1. Upon the addition of Fe^{3+} from 0 to 1.5 equiv to APSB solution, the fluorescence emission intensity
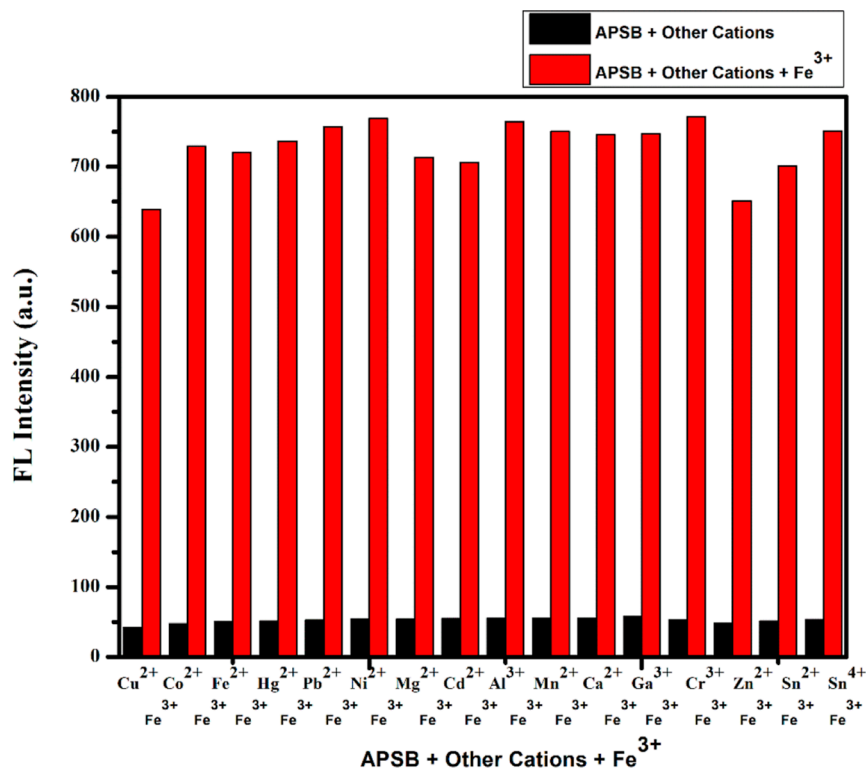
Figure 3. Competitive study of APSB−Fe^{3+} sensor over various metal ions in DMSO/water (95/5, v/v) solution, λ_{em} = 520 nm.
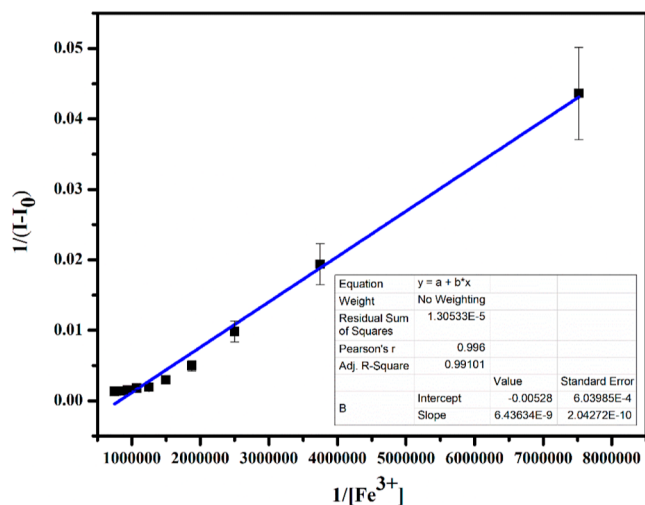

Figure 4. Benesi−Hildebrand plot of $1/(I_0 - I)$ vs $1/[Fe^{3+}]$ based on 1:1 stoichiometry between the sensor APSB−Fe^{3+} complex, λ_{em} = 520 nm.

Figure 5. Reversibility in fluorescence emission spectra of APSB (1×10^{-5} M) DMSO/water (95/5, v/v) solution with Fe^{3+} (1×10^{-3} M) and EDTA (2×10^{-3} M), λ_{em} = 520 nm.

increased gradually without affecting the peak position. UV/vis absorption spectrum showed a decrease in absorption peaks on the successive addition of Fe^{3+} (Figures S9 and S10, R^2 = 0.9923). The hypochromic shift was noticed from 375 to 430 nm, and the hyperchromic shift was observed at 270−285 nm in the absorption spectra. Besides, 7 nm of the hypochromic shift was also observed from 375 to 368 nm. These changes observed in the spectra suggested that the PET process was blocked in the complex. At a higher concentration of Fe^{3+} (above 1.5 equiv), the increase in absorption and emission intensities was stopped due to the saturation of complexation with the Fe^{3+} ion.
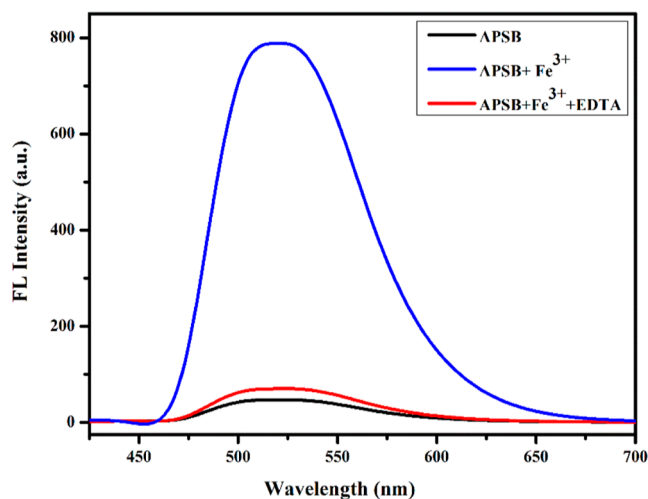
The fluorescent quantum yield calculations were performed for both APSB and APSB−Fe^{3+} using the relative quantum yield method which involves the use of a well characterized standard with a known quantum yield value. For this purpose, rhodamine 6G was used as the standard whose quantum yield value is 0.95 in ethanol. The quantum yields for APSB and APSB−Fe^{3+} have been calculated as 0.035 and 0.573, respectively, based on the equation given below.

$$Q.\,Y_S = Q.\,Y_R(I_S/I_R)[(1 - 10^{-AR})/(1 - 10^{-AS})](n_S/n_R)^2$$

where the subscripts S and R denote the sample and reference, respectively. $Q.Y_R$ is the known quantum yield (0.95 in ethanol) of the reference standard, I is the integral
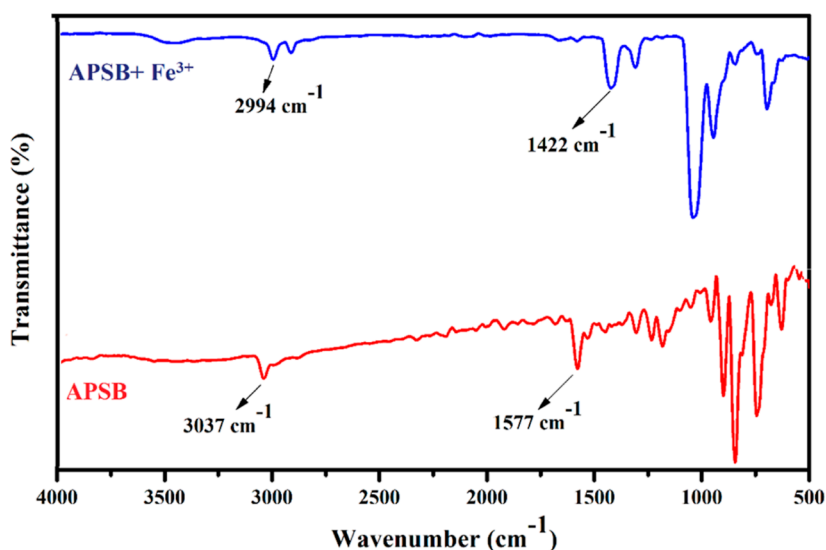
Figure 6. FT-IR spectra of APSB and APSB−Fe^{3+} (1:1) complex.
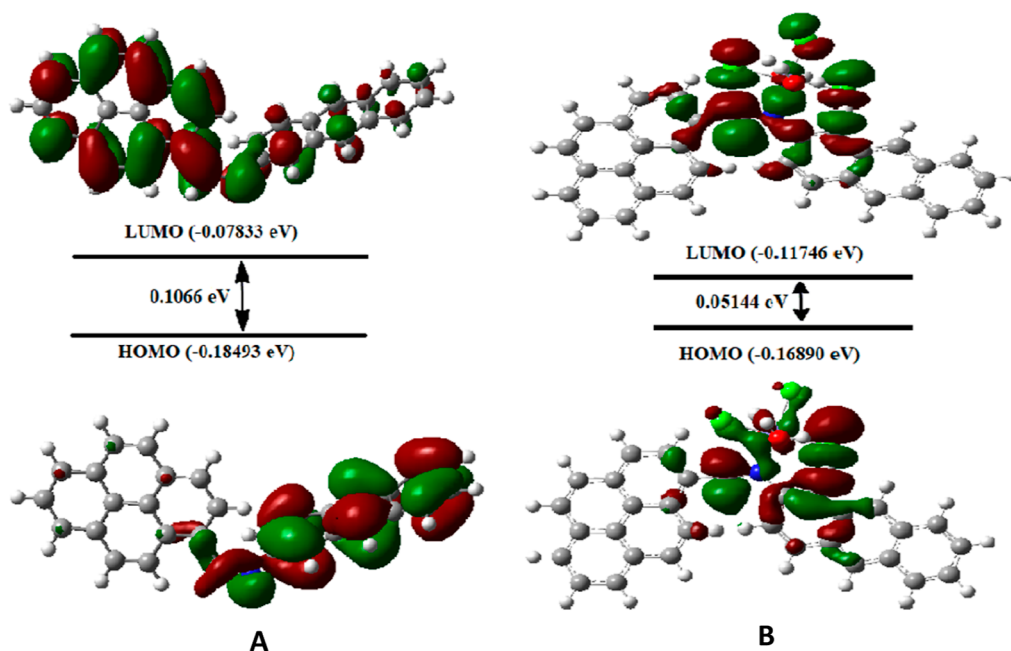

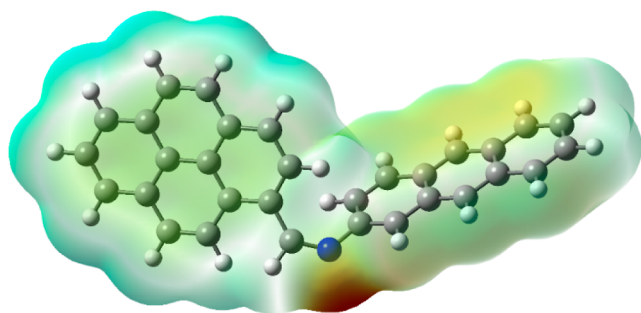**Figure 7.** HOMO−LUMO energy gap for APSB (A) and APSB−Fe^{3+} complex (B).

Figure 8. MEP of sensor APSB calculated using the B3LYP/6-311G(d,p) basis set.

fluorescence spectrum intensity, A is the absorbance of the solution at the excitation wavelength, and n is the refractive index of the solution solvent.[27]

Metal Ion Selectivity Study. To explore the metal ion selectivity of the sensor APSB over other different coexisting metal ions, a competitive study was carried out (Figure 2). The sensor APSB (1×10^{-5} M) and Fe^{3+} (1×10^{-3} M) with different metal ions including Co^{2+}, Cr^{3+}, Cu^{2+}, Fe^{2+}, Hg^{2+}, Pb^{2+}, Ga^{3+}, Ni^{2+}, Mg^{2+}, Cd^{2+}, Ca^{2+}, Mn^{2+}, Al^{3+}, Zn^{2+}, Sn^{2+}, and Sn^{4+} (1×10^{-3} M) in DMSO/water (95/5, v/v) medium were used for the fluorescence spectral studies. The results described that all selected metal ions did not affect Fe^{3+} binding to APSB, showing that the presence of other metal ions imparts insignificant interference to Fe^{3+} detection. These observations indicated that the sensor APSB can be used to detect Fe^{3+} in environmental and real sample analysis applications (Figure 3).

Binding Stoichiometry and Association Constant. The binding stoichiometry between APSB and Fe^{3+} was evaluated using the Job's plot method.[28] The sensor APSB and Fe^{3+} were taken in equal concentrations (1:1, 1×10^{-5} M) in
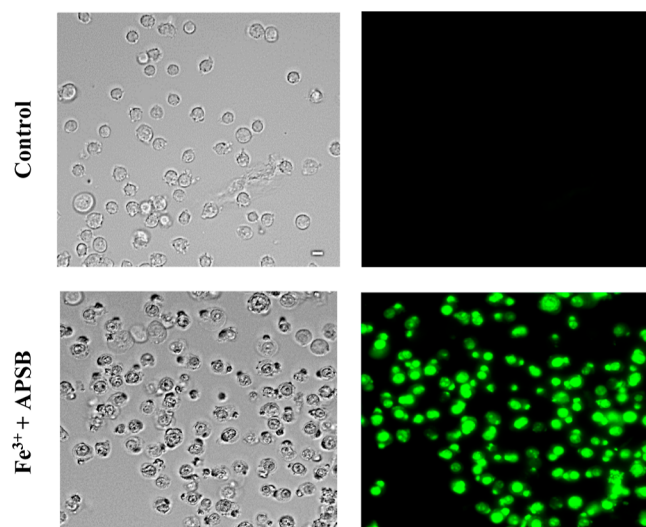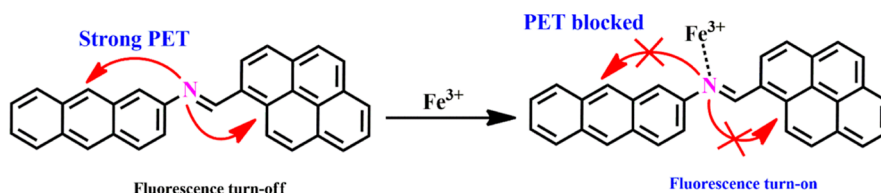
Scheme 2. Proposed PET Sensing Mechanism of APSB−Fe³⁺ Complex

Figure 9. Bio-imaging visualization of live HeLa cells toward the detection of Fe^{3+} ions (50 μM) with sensor APSB (10 μM).

DMSO/water (95/5, v/v) medium. The concentration of the sensor APSB varied from 0.1×10^{-5} to 1×10^{-5} M. The Job's plot described that the highest emission intensity was observed at 0.5 mol fractions (Figure S11), thereby confirming a 1:1 stoichiometry between the sensor APSB and the Fe^{3+} ion complex.

The 1:1 stoichiometry was further confirmed by the Benesi−Hildebrand plot as shown in Figure 4. The association constant was calculated from the fluorescence titration curve (Figure 1), and the value is found to be $K_a = 8.20 \times 10^5$ M^{-1}.[29] This result revealed that the binding between the sensor APSB and the Fe^{3+} ion was strong. UV−vis Benesi−Hildebrand plot was also used to confirm the 1:1 binding ratio between the sensor APSB and Fe^{3+} (Figure S12). The detection limit of the sensor APSB was determined based on the linear curve of emission data using the formula $3\sigma/K$. The detection limit value was found to be 1.95 nM. A better linear relationship was observed ($R^2 = 0.9892$) at 520 nm, showing a good linear correlation for the detection of a Fe^{3+} ion.

Reversibility of the Sensor APSB. We further investigated the reversibility behavior of the sensor APSB since it is very important when we consider its applications in the field of sensing and bioimaging. The APSB−Fe^{3+} complex (1×10^{-5} M^{-1} to 1×10^{-3} M) in DMSO/water (95/5, v/v) medium was reversed by EDTA addition (2.0×10^{-3} M). The Fe^{3+} complex formation with the sensor APSB disappeared after the addition of EDTA (Figure 5), revealing that the sensing action is reversible.
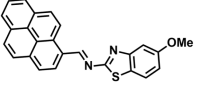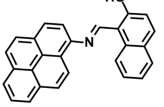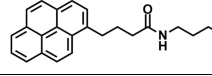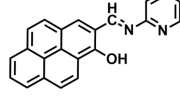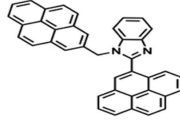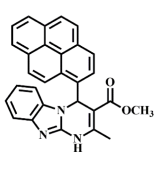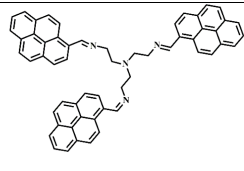
IR Spectral Analysis. To obtain a deep knowledge of the complex formation mechanism between the sensor APSB and Fe^{3+}, FT-IR spectral study was performed. As depicted in Figure 6, the IR peak of imine −C═N (1577 cm^{-1}) and

aromatic hydrogens (3037 cm^{-1}) appeared at their expected regions. Upon the addition of Fe^{3+} to APSB, the blue shift of peaks was observed from 1577 to 1422 and 3037 to 2994 cm^{-1} for imine −C═N and aromatic hydrogen moieties, respectively. The results obtained suggested the possible coordination of Fe^{3+} with the imine −C═N moiety. This coordination mechanism is also explained by hard−soft acid−base theory, and hard nitrogen centers selectively bind with hard metal Fe^{3+}.[30,31] Besides, Fe^{3+} is a strong Lewis acid; therefore, preferentially it tends to accept the lone pair electrons from the nitrogen of the imine group.[32] Therefore, the FT-IR results revealed the coordination of Fe^{3+} with APSB occurred between the imine −C═N group.

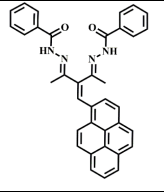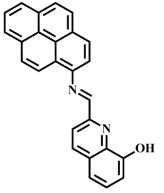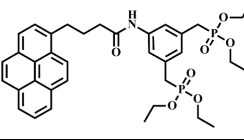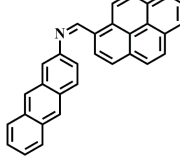**Electrochemical Study.** To have a better understanding of the binding mechanism of the sensor APSB with Fe^{3+}, cyclic voltammetry (CV) studies were performed in 1 mM PBS at a pH of 7 (Figure S13). Anodic peak current was observed at a scan rate of 0.1Vs-1 with reference to an Ag/AgCl electrode. Glassy carbon (GC) and platinum electrodes served as the working and counter electrodes, respectively.[33] On the bare GC, no characteristic redox peaks were observed. From the cyclic voltammogram of the modified electrode (GC/APSB), one oxidation peak was observed for the sensor APSB (1×10^{-5} M) at $E_{pa} = 0.255$ V. On the GC/APSB, the current density of the peak was suppressed since an insulating layer of the sensor APSB was formed on the modified working electrode.[34,35] On the GC/APSB−Fe^{3+}, a higher current density was observed for the peak in comparison to GC and GC/APSB electrodes, and the potential was shifted to $E_{pa} = 0.30$ V, which could be attributed to the larger conductivity of the Fe^{3+} membrane used along with the sensor APSB.[36] These outcomes indicate a strong binding affinity of the sensor APSB toward Fe^{3+} ions.

Theoretical Calculation Studies. The experimental results were validated by optimizing the molecular orbital geometry of the sensor APSB and its complex by B3LYP/6-311G and B3LYP/LANL2DZ level of theories using Gaussian 09 software. The optimized structures of the sensor APSB and the complex APSB−Fe^{3+} are shown in Figure S14. The DFT results indicate that the electron density of the sensor APSB is mainly distributed in the anthracene unit at HOMO, and for LUMO, the electron density is mainly located at the pyrene unit. It indicates that a strong PET process takes place. Upon the addition of Fe^{3+} with the imine nitrogen units of APSB, the PET process stops and exhibits significant fluorescent enhancement. It can be further explained as, after the addition of Fe^{3+} to the sensor APSB, the charge density in HOMO and LUMO energy levels was reallocated toward the Fe^{3+} ion. This result demonstrates, that the lone pair electron transferred from nitrogen atoms to the electron-deficient Fe^{3+} metal ion. Hence, due to this electron transfer, the PET process in the sensor APSB is stopped which leads to a significant enhancement in the fluorescent intensity (Figure 7).[37,38]

Table 1. Comparison of LOD Values of Previously Reported Pyrene-Based Compounds for Fe^{3+} with This work[47−56]

Sl.No	Fluorescent Probe	LOD (M)	Applications	Reference
1		2.61×10^{-6}	Detection of Ag^+ and Fe^{3+}	47
2		3.19×10^{-6}	Selective detection of Fe^{3+}	48
3		5.5×10^{-4}	Detection of Fe^{3+}	49
4		2.0×10^{-6}	Selective Fe^{3+} Ions Sensing	50
5		1.81×10^{-6}	Selective detection of Fe^{3+}	51
6		7.94×10^{-6}	Selective recognition of Zn^{2+} in organic and Fe^{3+} in aqueous medium	52
7		336×10^{-9}	In vitro bioimaging, protein binding studies and detection of bilirubin and Fe^{3+}	53
8		1.67×10^{-6}	Detection of Fe^{3+} and Fe^{2+} Ions and its Application in Live Cell Imaging	54
9		2.52×10^{-8}	Selective Detection of Fe^{3+} with Logic Gate Application	55
10		0.99×10^{-6}	Selective Fe^{3+} Ions Sensing	56
11		1.95×10^{-9}	-	Present Wok

Generally, the MEP surface analysis provides information regarding the three-dimensional charge distributions of molecules. When correlated with a dipole moment, partial charges, electronegativity, and chemical reactivity sites found in the molecule, MEP shows significant traits including variation in electron density, size, and form.[39−42] MEP analysis reveals the electron-rich and deficient areas of the molecules, and therefore the molecule's sites available for the electrophilic attack can be efficiently identified by MEP analysis.[43] This surface analysis helps to visualize differently charged regions of the molecules which are indicated by different colors. The surface analysis result obtained by molecular electrostatic analysis is given in Figure 8. Analyzing the positive and negative charged electrostatic potential regions in the compound allows for the prediction of various potential interactions in the molecules. The absence of electrons or the partial positive charge that the molecule possesses is described by the surface with high electrostatic potential, which is depicted by the color blue.[44] The MEP surface reveals that the region near the nitrogen atom is highly sensitive to electrophilic attacks. This study also describes the possibility of a strong interaction between imine nitrogen of the sensor APSB and the Fe^{3+} ion.

Proposed Binding Mechanism. Based on the spectroscopy study results such as ^1H NMR, FT-IR, ^{13}C NMR, and theoretical investigations including DFT studies, here we propose a plausible binding mechanism for the APSB−Fe^{3+} complex. In the sensor APSB, a strong PET process caused a weak fluorescence intensity; on the other hand, the addition of Fe^{3+} which formed an interaction with −C=N moiety resulted in a weak PET process and significant improvement in fluorescent emission. The interaction established between the sensor APSB and Fe^{3+} complex obstructs the PET pathways (Scheme 2).

Fluorescence Imaging in Living Cells. At last, to examine the practical application of the sensor APSB for the selective detection of Fe^{3+} in living cells, a fluorescence imaging study was carried out. Biocompatibility of the compound always attains first consideration when performing live-cell imaging studies. So, the sensor APSB was tested for its cytotoxicity against HeLa cells using an MTT assay. To perform this, first, the cells were incubated with various concentrations (0, 10, 20, 30, 40, and 50 μM) of the sensor APSB for 48 h at 37 °C.[45,46] The results of this study indicated the nontoxic behavior of the sensor APSB toward the cultured cells. Also, the sensor is not imparting any dreadful effect on the cell viability even at its higher concentration (50 μM), which clearly shows the ability of the sensor APSB to detect Fe^{3+} ions in live and active HeLa cells. The cell imaging studies were carried out using the sensor APSB, and the fluorescence images of HeLa cells were recorded using a fluorescence microscope. The results (Figure 9) convey that the treatment of the sensor APSB (5 μM) with the cells for this does not show any fluorescence due to its very weak fluorescence property. However, the treatment of the sensor APSB along with Fe^{3+} ions shows significant fluorescence in HeLa cells. The fluorescence images of the cells were captured using a fluorescence microscope, and the results further indicated that the sensor APSB is cell-permeable and possesses a high ability to monitor Fe^{3+} ions in living cells.

The sensor APSB exhibited in this work is also compared with other chemosensors reported previously (Table 1). The comparison study reveals that the present sensor APSB exhibits
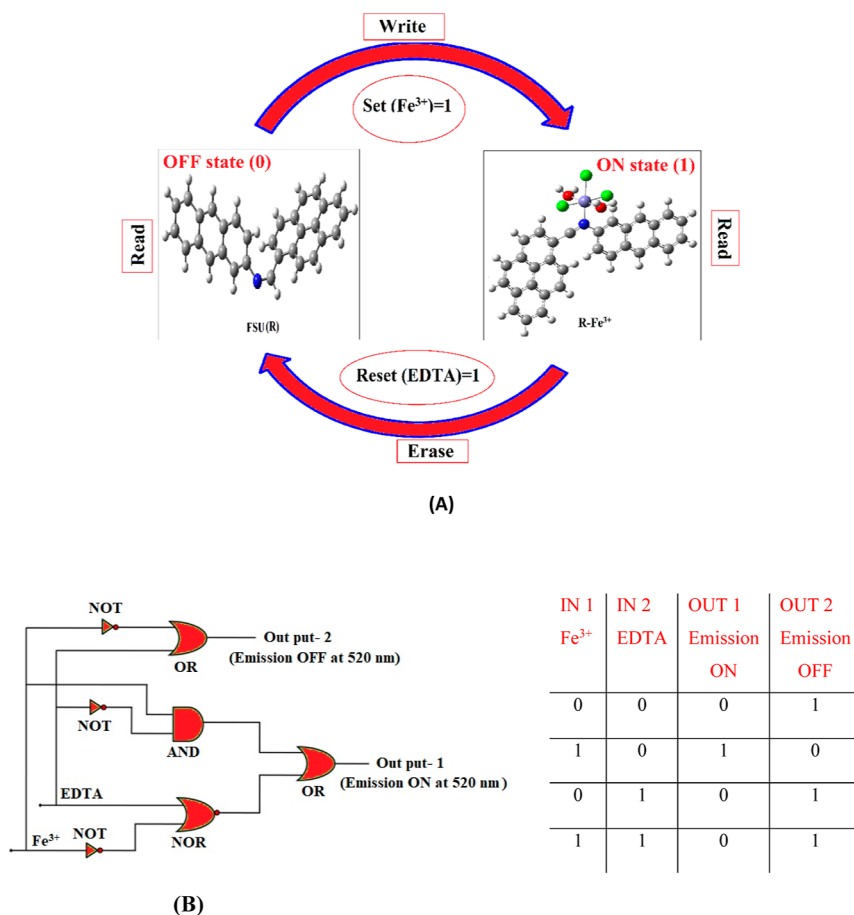
Figure 10. A memory device that contains a loop with Write−Read−Erase−Read functions explaining the reversible logic gate operations (A) and logic gate circuit and its truth table (B).

an appreciable detection limit. Similarly, the sensor shows better performance in fluorescence live-cell imaging studies. Therefore, it is highlighted that the present sensor APSB could play a better role in the field of analytical chemistry for the detection of Fe^{3+} ions with a low detection limit without the interference of other metal ions.

Molecular Logic Gate Application. The development of molecular switches that are reversible has gained significant importance in the present world where information technology is growing tremendously. In this present study, we also constructed a logic gate to obtain molecular-level information by using the fluorescence system described in this work (Figure 10). Fe^{3+} and EDTA were the two chemical inputs employed in the logic gate system for the set and reset that are designated as S and R. When Fe^{3+} is present, the input is high and the system will be in an ON state that can be memorized as 1 binary state. When EDTA is present (high reset input), the OFF state denoted by the binary state 0 is activated automatically by deleting the ON written information. Apart from this, the selective detection of Fe^{3+} and EDTA together with the reversible switching function of the chemosensor FSU brings a way to develop a truth table and suggests Boolean logic gates at the molecular level. As described in Figure 10, the input signals such as Fe^{3+} and EDTA are represented using the Boolean expressions 0 and 1. On the other hand, strong fluorescence emission at 520 nm was denoted as 1 (ON mode), and 0 (OFF mode) represents the loss of fluorescence property of the chemosensor FSU. The truth table has been

constructed completely based on the fluorescence emission data obtained from the spectrofluorometer. The molecular logic gate described here is associated with OR, AND, NOT NOR, and NAND gates. Based on the truth table, it is clear that the chemosensor FSU precisely mimicked the logic gate constructed in this work. In summary, the logic gate system gives intense fluorescence emission only when the input is Fe^{3+} (1,0), and all other possible input combinations provide extremely low fluorescence emission OFF or 0.

■ CONCLUSIONS

In summary, a novel pyrene-based sensor was synthesized and characterized by ^{1}H NMR, ^{13}C NMR, ESI-MS, and spectroscopic studies. This study shows that the sensor APSB is highly selective and sensitive toward Fe^{3+} ion detection. This sensor exhibits a turn-on fluorescence response toward Fe^{3+} and shows a strong fluorescence emission at 520 nm with a remarkable (17-fold) enhancement in fluorescence intensity. The detection limit value was 1.95 nM, and the binding constant value was obtained as 8.20×10^5 M^{-1}. The fluorescence quantum yields for APSB and APSB−Fe^{3+} were calculated as 0.035 and 0.573, respectively. The Fe^{3+} ion sensing by the sensor APSB involves a PET mechanism, which is also supported by DFT studies and FT-IR spectral studies. The cell viability study described that a lower concentration of the sensor APSB was not interfering with the normal cellular functions. A fluorescence imaging study demonstrated the permeability of APSB in cell walls and the effective sensing of

Fe^{3+} inside the HeLa cells. Furthermore, the EDTA study revealed the reversibility nature and reusability of the developed sensor APSB.

ASSOCIATED CONTENT

Supporting Information

The Supporting Information is available free of charge at https://pubs.acs.org/doi/10.1021/acsomega.2c03718.

> Synthetic procedures, NMR spectra, mass spectra, linear response of fluorescence titration of APSB, solvatochromic studies of compound APSB, time-dependence study, effect of pH on receptor APSB, UV−vis spectral studies of APSB with metal ions, Job's plot, CV of APSB, and proposed optimized geometries of APSB and its Fe^{3+} complex (PDF)

AUTHOR INFORMATION

Corresponding Author

Anandaram Sreekanth − *Department of Chemistry, National Institute of Technology-Tiruchirappalli, 620015 Tiruchirappalli, Tamil Nadu, India;* ⊙ orcid.org/0000-0002-2942-8487; Phone: +91 431 2503642; Email: sreekanth@nitt.edu; Fax: +91 431 2500133

Authors

Puthiyavalappil Rasin − *Department of Chemistry, National Institute of Technology-Tiruchirappalli, 620015 Tiruchirappalli, Tamil Nadu, India*

Vipin Manakkadan − *Department of Chemistry, National Institute of Technology-Tiruchirappalli, 620015 Tiruchirappalli, Tamil Nadu, India*

Vishnunarayanan Namboothiri Vadakkedathu Palakkeezhillam − *Department of Chemistry, National Institute of Technology-Tiruchirappalli, 620015 Tiruchirappalli, Tamil Nadu, India*

Jebiti Haribabu − *Facultad de Medicina, Universidad de Atacama, 1532502 Copiapo, Chile;* ⊙ orcid.org/0000-0001-8855-032X

Cesar Echeverria − *Facultad de Medicina, Universidad de Atacama, 1532502 Copiapo, Chile*

Complete contact information is available at:
https://pubs.acs.org/10.1021/acsomega.2c03718

Notes

The authors declare no competing financial interest.

ACKNOWLEDGMENTS

REFERENCES

(1) Catherine Nyona Malele, B.Design, synthesis and photophysics of dipyrrolequinoxaline receptor loaded fluorescent conjugated polymer. Ph.D. thesis, State University of New York at Binghamton; ProQuest Dissertations Publishing, 2009, p 3372312.

(2) Choudhury, N.; Saha, B.; De, P. Recent Progress in Polymer-Based Optical Chemosensors for Cu^{2+} and Hg^{2+} Ions: A Comprehensive Review. *Eur. Polym. J.* **2021**, *145*, 110233.

(3) Hishimone, P. N.; Hamukwaya, E.; Uahengo, V. The C 2-Symmetry Colorimetric Dye Based on a Thiosemicarbazone Derivative and Its Cadmium Complex for Detecting Heavy Metal Cations (Ni^{2+}, Co^{2+}, Cd^{2+}, and Cu^{2+}) Collectively, in DMF. *J. Fluoresc.* **2021**, *31*, 999−1008.

(4) Lim, J. W.; Kim, T. Y.; Woo, M. A. Trends in Sensor Development toward Next-Generation Point-of-Care Testing for Mercury. *Biosens. Bioelectron.* **2021**, *183*, 113228.

(5) Xu, Z.; Chen, J.; Liu, Y.; Wang, X.; Shi, Q. Multi-Emission Fluorescent Sensor Array Based on Carbon Dots and Lanthanide for Detection of Heavy Metal Ions under Stepwise Prediction Strategy. *Chem. Eng. J.* **2022**, *441*, 135690.

(6) Shyamal, M.; Maity, S.; Maity, A.; Maity, R.; Roy, S.; Misra, A. Aggregation Induced Emission Based "Turn-off" Fluorescent Chemosensor for Selective and Swift Sensing of Mercury (II) Ions in Water. *Sens. Actuators, B* **2018**, *263*, 347−359.

(7) Chowdhury, S.; Rooj, B.; Dutta, A.; Mandal, U. Review on Recent Advances in Metal Ions Sensing Using Different Fluorescent Probes. *J. Fluoresc.* **2018**, *28*, 999−1021.

(8) Tarai, A.; Li, Y.; Liu, B.; Zhang, D.; Li, J.; Yan, W.; Zhang, J.; Qu, J.; Yang, Z. A Review on Recognition of Tri-/Tetra-Analyte by Using Simple Organic Colorimetric and Fluorometric Probes. *Coord. Chem. Rev.* **2021**, *445*, 214070.

(9) Kasozi, N.; Tandlich, R.; Fick, M.; Kaiser, H.; Wilhelmi, B. Iron Supplementation and Management in Aquaponic Systems: A Review. *Aquacult. Rep.* **2019**, *15*, 100221.

(10) Sundararajan, S.; Rabe, H. Prevention of Iron Deficiency Anemia in Infants and Toddlers. *Pediatr. Res.* **2021**, *89*, 63−73.

(11) Pivina, L.; Semenova, Y.; Doşa, M. D.; Dauletyarova, M.; Bjørklund, G. Iron Deficiency, Cognitive Functions, and Neurobehavioral Disorders in Children. *J. Mol. Neurosci.* **2019**, *68*, 1−10.

(12) Vona, R.; Pallotta, L.; Cappelletti, M.; Severi, C.; Matarrese, P. The Impact of Oxidative Stress in Human Pathology: Focus on Gastrointestinal Disorders. *Antioxidants* **2021**, *10*, 201.

(13) Turan, B. A Brief Overview from the Physiological and Detrimental Roles of Zinc Homeostasis via Zinc Transporters in the Heart. *Biol. Trace Elem. Res.* **2019**, *188*, 160−176.

(14) Bhutani, P.; Joshi, G.; Raja, N.; Bachhav, N.; Rajanna, P. K.; Bhutani, H.; Paul, A. T.; Kumar, R. U.S. FDA Approved Drugs from 2015-June 2020: A Perspective. *J. Med. Chem.* **2021**, *64*, 2339−2381.

(15) Islam, M. M.; Hu, Z.; Wang, Q.; Redshaw, C.; Feng, X. Pyrene-Based Aggregation-Induced Emission Luminogens and Their Applications. *Mater. Chem. Front.* **2019**, *3*, 762−781.

(16) Shaya, J.; Corridon, P. R.; Al-Omari, B.; Aoudi, A.; Shunnar, A.; Mohideen, M. I. H.; Qurashi, A.; Michel, B. Y.; Burger, A. Design, Photophysical Properties, and Applications of Fluorene-Based Fluorophores in Two-Photon Fluorescence Bioimaging: A Review. *J. Photochem. Photobiol., C* **2022**, *52*, 100529.

(17) Lyu, Y.; Pu, K. Recent Advances of Activatable Molecular Probes Based on Semiconducting Polymer Nanoparticles in Sensing and Imaging. *Adv. Sci.* **2017**, *4*, 1600481.

(18) Lawal, A. T. Graphene-Based Nano Composites and Their Applications. A Review. *Biosens. Bioelectron.* **2019**, *141*, 111384.

(19) Jamkhande, P. G.; Ghule, N. W.; Bamer, A. H.; Kalaskar, M. G. Metal Nanoparticles Synthesis: An Overview on Methods of Preparation, Advantages and Disadvantages, and Applications. *J. Drug Delivery Sci. Technol.* **2019**, *53*, 101174.

(20) Chavada, V. D.; Bhatt, N. M.; Sanyal, M.; Shrivastav, P. S. Dual Fluorescence-Colorimetric Silver Nanoparticles Based Sensor for Determination of Olanzapine: Analysis in Rat Plasma and Pharmaceuticals. *J. Fluoresc.* **2020**, *30*, 955−967.

(21) Singh, R.; Majhi, S.; Sharma, K.; Ali, M.; Sharma, S.; Choudhary, D.; Tripathi, C. S. P.; Guin, D. BSA Stabilized Copper Nanoclusters as a Highly Sensitive and Selective Probe for Fluorescence Sensing of Fe^{3+} Ions. *Chem. Phys. Lett.* **2022**, *787*, 139226.

(22) Zheng, T.; Xu, Z.; Zhao, Y.; Li, H.; Jian, R.; Lu, C. Multiresponsive Polysiloxane Bearing Photochromic Spirobenzopyran for Sensing PH Changes and Fe3+ Ions and Sequential Sensing of Ag + and Hg2+ Ions. *Sens. Actuators, B* **2018**, *255*, 3305−3315.

(23) Haribabu, J.; Garisetti, V.; Malekshah, R. E.; Srividya, S.; Gayathri, D.; Bhuvanesh, N.; Mangalaraja, R. V.; Echeverria, C.;

Karvembu, R. Design and Synthesis of Heterocyclic Azole Based Bioactive Compounds: Molecular Structures, Quantum Simulation, and Mechanistic Studies through Docking as Multi-Target Inhibitors of SARS-CoV-2 and Cytotoxicity. *J. Mol. Struct.* **2022**, *1250*, 131782.

(24) Freimoser, F. M.; Jakob, C. A.; Aebi, M.; Tuor, U. The MTT [3-(4,5-Dimethylthiazol-2-Yl)-2,5-Diphenyltetrazolium Bromide] Assay Is a Fast and Reliable Method for Colorimetric Determination of Fungal Cell Densities. *Appl. Environ. Microbiol.* **1999**, *65*, 3727−3729.

(25) Carreño, E. A.; Alberto, A. V. P.; de Souza, C. A. M.; de Mello, H. L.; Anastacio Alves, A.; Alves, L. A. Considerations and Technical Pitfalls in the Employment of the MTT Assay to Evaluate Photosensitizers for Photodynamic Therapy. *Appl. Sci.* **2021**, *11*, 2603.

(26) Ozutsumi, K.; Kurihara, M.; Kawashima, T. structure of iron(ii1) ion and its complexation with thiocyanate ion in n,n-dimethylformamide. *Talanta* **1993**, *40*, 599−607.

(27) Nawara, K.; Waluk, J. Improved Method of Fluorescence Quantum Yield Determination. *Anal. Chem.* **2017**, *89*, 8650−8655.

(28) Zhang, X.; Shen, L. Y.; Zhang, Q. L.; Yang, X. J.; Huang, Y. L.; Redshaw, C.; Xu, H. A Simple Turn-off Schiff Base Fluorescent Sensor for Copper (II) Ion and Its Application in Water Analysis. *Molecules* **2021**, *26*, 1233.

(29) Stojanovic, N.; Murphy, L. D.; Wagner, B. D. Fluorescence-Based Comparative Binding Studies of the Supramolecular Host Properties of PAMAM Dendrimers Using Anilinonaphthalene Sulfonates: Unusual Host-Dependent Fluorescence Titration Behavior. *Sensors* **2010**, *10*, 4053−4070.

(30) Yuan, Y.; Yu, J.; Chen, H.; Bang, K.-T.; Pan, D.; Kim, Y. Thiol-Functionalized Zr Metal-Organic Frameworks for Efficient Removal of Fe3+ from Water. *Cell Rep. Phys. Sci.* **2022**, *3*, 100783.

(31) Irto, A.; Cardiano, P.; Chand, K.; Cigala, R. M.; Crea, F.; De Stefano, C.; Santos, M. A. Bifunctional 3-Hydroxy-4-Pyridinones as Potential Selective Iron(Iii) Chelators: Solution Studies and Comparison with Other Metals of Biological and Environmental Relevance. *Molecules* **2021**, *26*, 7280.

(32) Johnson, A. D.; Curtis, R. M.; Wallace, K. J. Low Molecular Weight Fluorescent Probes (LMFPs) to Detect the Group 12 Metal Triad. *Chemosensors* **2019**, *7*, 22.

(33) Mazurków, J. M.; Kusior, A.; Radecka, M. Electrochemical Characterization of Modified Glassy Carbon Electrodes for Non-enzymatic Glucose Sensors. *Sensors* **2021**, *21*, 7928.

(34) Jerez-Masaquiza, M. D.; Fernández, L.; González, G.; Montero-Jiménez, M.; Espinoza-Montero, P. J. Electrochemical Sensor Based on Prussian Blue Electrochemically Deposited at ZrO2 Doped Carbon Nanotubes Glassy Carbon Modified Electrode. *Nanomaterials* **2020**, *10*, 1328.

(35) Shinwari, M.; Zhitomirsky, D.; Deen, I. A.; Selvaganapathy, P. R.; Deen, M.; Landheer, D. Microfabricated Reference Electrodes and Their Biosensing Applications. *Sensors* **2010**, *10*, 1679−1715.

(36) Bressi, V.; Akbari, Z.; Montazerozohori, M.; Ferlazzo, A.; Iannazzo, D.; Espro, C.; Neri, G. On the Electroanalytical Detection of Zn Ions by a Novel Schiff Base Ligand-SPCE Sensor. *Sensors* **2022**, *22*, 900.

(37) de Silva, A. P.; Moody, T. S.; Wright, G. D. Fluorescent PET (Photoinduced Electron Transfer) Sensors as Potent Analytical Tools. *Analyst* **2009**, *134*, 2385−2393.

(38) Daly, B.; Ling, J.; de Silva, A. P. Current Developments in Fluorescent PET (Photoinduced Electron Transfer) Sensors and Switches. *Chem. Soc. Rev.* **2015**, *44*, 4203−4211.

(39) Halim, S. A.; Ibrahim, M. A. Synthesis, FT-IR, Structural, Thermochemical, Electronic Absorption Spectral, and NLO Analysis of the Novel 10-Methoxy-10: H -Furo[3,2- g] Chromeno[2,3- b] [1,3]Thiazolo[5,4- e] Pyridine-2,10(3 H)-Dione (MFCTP): A DFT/TD-DFT Study. *RSC Adv.* **2021**, *11*, 32047−32066.

(40) Pokharia, S.; Joshi, R.; Pokharia, M.; Yadav, S. K.; Mishra, H. A Density Functional Theory Insight into the Structure and Reactivity of Diphenyltin(IV) Derivative of Glycylphenylalanine. *Main Group Met. Chem.* **2016**, *39*, 77−86.

(41) Uzzaman, M.; Shawon, J.; Siddique, Z. A. Molecular Docking, Dynamics Simulation and ADMET Prediction of Acetaminophen and Its Modified Derivatives Based on Quantum Calculations. *SN Appl. Sci.* **2019**, *1*, 1783.

(42) Oliveira, L. F. S. d.; Cordeiro, H. C.; Brito, H. G. d.; Pinheiro, A. C. B.; Santos, M. A. B. d.; Bitencourt, H. R.; Figueiredo, A. F. d.; Araújo, J.; de, J. O.; Gil, F.; dos, S.; Farias, M. d. S.; Barbosa, J. P.; Pinheiro, J. C. Molecular Electrostatic Potential and Pattern Recognition Models to Design Potentially Active Pentamidine Derivatives against Trypanosoma Brucei Rhodesiense. *Res. Soc. Dev.* **2021**, *10*, No. e261101220207.

(43) Djebaili, R.; Melkemi, N.; Kenouche, S.; Daoud, I.; Bouachrine, M.; Hazhazi, H.; Salah, T. Combined Conceptual-Dft, Quantitative Mep Analysis, and Molecular Docking Study of Benzodiazepine Analogs. *Orbital* **2021**, *13*, 301−315.

(44) Haji-Ghassemi, O.; Blackler, R. J.; Martin Young, N. M.; Evans, S. V. Antibody Recognition of Carbohydrate Epitopes. *Glycobiology* **2015**, *25*, 920−952.

(45) Kavitha, V.; Ramya, M.; Viswanathamurthi, P.; Haribabu, J.; Echeverria, C. Design of a Dual Responsive Receptor with Oxochromane Hydrazide Moiety to Monitor Toxic Hg2+ and Cd2+ Ions: Usage on Real Samples and Live Cells. *Environ. Pollut.* **2022**, *301*, 119036.

(46) Asaithambi, G.; Periasamy, V.; Jebiti, H. Near-Infrared Fluorogenic Receptor for Selective Detection of Cysteine in Blood Serum and Living Cells. *Anal. Bioanal. Chem.* **2021**, *413*, 1817−1826.

(47) Zhang, W.; Luo, Y.; Zhou, Y.; Liu, M.; Xu, W.; Bian, B.; Tao, Z.; Xiao, X. A Highly Selective Fluorescent Chemosensor Probe for Detection of Fe3+ and Ag+ Based on Supramolecular Assembly of Cucurbit[10]Uril with a Pyrene Derivative. *Dyes Pigm.* **2020**, *176*, 108235.

(48) Aigner, D.; Freunberger, S. A.; Wilkening, M.; Saf, R.; Borisov, S. M.; Klimant, I. Enhancing Photoinduced Electron Transfer Efficiency of Fluorescent PH-Probes with Halogenated Phenols. *Anal. Chem.* **2014**, *86*, 9293−9300.

(49) Doust Mohammadi, M.; Abdullah, H. Y. The Adsorption of Bromochlorodifluoromethane on Pristine and Ge-Doped Silicon Carbide Nanotube: A PBC-DFT, NBO, and QTAIM Study. *Struct. Chem.* **2021**, *32*, 481−494.

(50) Adole, V. A. Computational Chemistry Approach for the Investigation of Structural, Electronic, Chemical and Quantum Chemical Facets of Twelve Biginelli Adducts. *Appl. Organomet. Chem.* **2021**, *1*, 29−40.

(51) Rasin, P.; Mathew, M. M.; Manakkadan, V.; Palakkeezhillam, V. N. V.; Sreekanth, A. A Highly Fluorescent Pyrene-Based Sensor for Selective Detection Of Fe3+ Ion in Aqueous Medium: Computational Investigations. *J. Fluoresc.* **2022**, *32*, 1229−1238.

(52) Raj, T.; Saluja, P.; Singh, N. A New Class of Pyrene Based Multifunctional Chemosensors for Differential Sensing of Metals in Different Media: Selective Recognition of Zn2+ in Organic and Fe3+ in Aqueous Medium. *Sens. Actuators, B* **2015**, *206*, 98−106.

(53) Srinivasan, V.; Jhonsi, M. A.; Dhenadhayalan, N.; Lin, K. C.; Ananth, D. A.; Sivasudha, T.; Narayanaswamy, R.; Kathiravan, A. Pyrene-Based Prospective Biomaterial: In Vitro Bioimaging, Protein Binding Studies and Detection of Bilirubin and Fe3+. *Spectrochim. Acta, Part A* **2019**, *221*, 117150.

(54) Dhivya, R.; Gomathi, A.; Viswanathamurthi, P. Pyrene Based Fluorescent Turn-on Chemosensor for Sequential Detection of Fe3+ and Fe2+ Ions and Its Application in Live Cell Imaging. *J. Fluoresc.* **2019**, *29*, 797−802.

(55) Mukherjee, S.; Talukder, S. A Reversible Pyrene-Based Turn-on Luminescent Chemosensor for Selective Detection of Fe3+ in Aqueous Environment with Logic Gate Application. *J. Fluoresc.* **2016**, *26*, 1021−1028.

(56) Padghan, S. D.; Bhosale, R. S.; Bhosale, S. V.; Antolasic, F.; Al Kobaisi, M.; Bhosale, S. V. Pyrene-Phosphonate Conjugate: Aggregation-Induced Enhanced Emission, and Selective Fe3+ Ions Sensing Properties. *Molecules* **2017**, *22*, 1417.